JCTC Journal of Chemical Theory and Computation

Article

pubs.acs.org/JCTC

The Effect of Newly Developed OPLS-AA Alanyl Radical Parameters on Peptide Secondary Structure

Michael C. Owen,[†,§,∥,⊥] László Tóth,[#] Balázs Jójárt,[§,⊥] István Komáromi,[#] Imre G. Csizmadia,[†,‡,§,∥,⊥] and Bela Viskolcz*[,§,⊥]

[†]Materials Science Research Institute, Faculty of Dentistry, Semmelweis University, Üllöi út 26. H-1085 Budapest, Hungary

[‡]Department of Chemistry, University of Toronto, Toronto, Ontario M5S 3H6, Canada

[§]Department of Chemical Informatics, Faculty of Education, University of Szeged, Boldogasszony sgt. 6, H-6725 Szeged, Hungary

[∥]Global Institute of Computational Molecular and Materials Science (www.giocomms.org)

[⊥]Drug Discovery Research Center (www.drugcent.com)

[#]Thrombosis and Haemostasis Research Group of the Hungarian Academy of Sciences at the University of Debrecen, H-4010, Hungary

Supporting Information

ABSTRACT: Recent studies using ab initio calculations have shown that C_α-centered radical formation by H-abstraction from the backbone of peptide residues has dramatic effects on peptide structure and have suggested that this reaction may contribute to the protein misfolding observed in Alzheimer's and Parkinson's diseases. To enable the effects of C_α-centered radicals to be studied in longer peptides and proteins over longer time intervals, force-field parameters for the C_α-centered Ala radical were developed for use with the OPLS force field by minimizing the sum of squares deviation between the quantum chemical and OPLS-AA energy hypersurfaces. These parameters were used to determine the effect of the C_α-centered Ala radical on the structure of a hepta-alanyl peptide in molecular dynamics (MD) simulations. A negligible sum-of-squares energy deviation was observed in the stretching parameters, and the newly developed OPLS-AA torsional parameters showed a good agreement with the LMP2/cc-pVTZ(-f) hypersurface. The parametrization also demonstrated that derived force-field bond length and bond angle parameters can deviate from the quantum chemical equilibrium values, and that the improper torsional parameters should be developed explicitly with respect to the coupled torsional parameters. The MD simulations showed planar conformations of the C_α-containing residue (Alr) are preferred and these conformations increase the formation of γ-, α-, and π-turn structures depending on the position in the turn occupied by the Alr residue. Higher-ordered structures are destabilized by Alr except when this residue occupies position "i + 1" of the 3_{10}-helix. These results offer new insight into the protein-misfolding mechanisms initiated by H-abstraction from the C_α of peptide and protein residues.

1. INTRODUCTION

Knowledge of the oxidative damage to proteins by free radicals has now become widespread. Free radicals have been shown to denature proteins, induce protein aggregation, and induce protein degradation.[1,2] They have also been shown to cause a loss in cellular function and apoptosis. Free radicals have been shown to play a role in several diseases, particularly Alzheimer's disease and other diseases associated with the misfolding of amyloid peptides.[3−7] These normally soluble peptides aggregate to form amyloid fibrils and amyloid plaques.[8,9] During this aggregation, it has been shown that an α to β conformational transition occurs and the β conformation has also been shown to be the most stable conformation for aggregated amyloid peptides.[10,11] Recent quantum chemical studies of pentapeptides have shown that peptide helices with C_α-centered radicals have a higher propensity to unfold to the β conformation than peptides with closed-shell electron configurations.[12,13]

Quantum chemical calculations have been shown to elucidate mechanisms of free radical-initiated oxidation of amino acids and peptide analogues.[14−20] One of many peptide radical structures and reaction intermediates, the C_α-centered radical is of particular interest because it is common to all of the amino acid residues and is stabilized by the capto-dative effect.[21−23] This oxidative step is initiated by OH-dependent abstraction of a hydrogen atom from the C_α of a peptide or protein.[24] A molecule such as H_2O_2 can provide the hydrogen atom to restore the L-configuration of the residue, or epimerization can occur.[25] The number of atoms contained in pentapeptides is near the upper limit for quantum chemical studies, and this technique is best-applied near potential energy critical points, using time-independent techniques. To determine the effect of C_α-centered radicals on the structure of large and dynamic systems, it would be useful to use force fields, particularly if one wishes to study the aggregation of multiple peptides or even proteins.

Unfortunately, radical force-field parameters are usually omitted from the standard parameters set for biological force fields such as AMBER, CHARMM, and OPLS-AA.[26−28] The continuously increasing knowledge of biochemical reaction mechanisms in which radicals are involved highlights the need

Received: January 27, 2012
Published: June 18, 2012

dx.doi.org/10.1021/ct300059f | J. Chem. Theory Comput. 2012, 8, 2569−2580

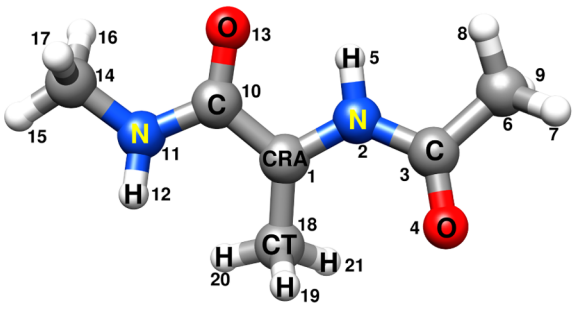

Bond lengths:

1	-2:	1.378;	2	-3:	1.384;	3	-4:	1.233;
2	-5:	1.018;	1	-10:	1.463;	10	-11:	1.367;
11	-12:	1.007;	10	-13:	1.254;	1	-18:	1.491;
18	-19:	1.092;	18	-20:	1.089;	18	-21:	1.088

Bond angles:

1	-2	-3:	128.0;	1	-2	-5:	112.1;	2	-3	-4:	123.1;
3	-2	-5:	119.2;	1	-10	-11:	117.6;	1	-10	-13:	120.8;
10	-11	-12:	118.4;	11	-10	-13:	121.5;	2	-1	-18:	122.3;
10	-1	-18:	126.2;	1	-18	-19:	112.4;	1	-18	-20:	110.0;
1	-18	-21:	110.4								

Torsion angles:

1	-2	-3	-4:	0.2;	1	-10	-11	-12:	17.5;
3	-2	-1	-18:	-18.2;	11	-10	-1	-18:	5.2;
13	-10	-1	-18:	-172.9;	5	-2	-1	-18:	171.7;
2	-1	-18	-19:	82.8;	2	-1	-18	-20:	-155.3;
2	-1	-18	-21:	-36.0					

UMP2 energy: -493.7943937 a.u.

Figure 1. The numbering of atoms in *N*-Ac-Ala$^{\bullet}$-NHMe residue used in calculations. The methyl hydrogen (H), methyl carbon (CT), C_α (CRA), amide nitrogen (N), and hydrogen (H) as well as the carbonyl carbon (C) and oxygen (O) atom types are labeled. Representative geometry parameters around the radical center are shown as well.

for the development of force-field parameters for amino acid residues containing a C_α-centered radical.[29−34] Quantum chemically derived force fields are practical because they enable transiently stable structures such as radicals to be studied. Lifson and Warshel proposed general equations to derive a fitted parameter set.[35] This method can be used to develop an optimal, that is, least-squares-fitted, parameter set based on a particular group of properties by using the derivatives of these properties with respect to the parameter set.[35] Numerous examples for this systematic parameter fitting based on either experimental quantities and/or quantum chemical calculations can be found in the literature.[35−45] This approach will be used to herein to expand the OPLS-AA force field parameter set to include the C_α-centered Ala radical.

The OPLS-AA force field is a Class I force field according to the generally accepted force-field classification criteria and is widely accepted for simulations of structures of peptides and proteins in solution.[28,46−49] It contains a general three-Fourier term torsional potential and special library for torsional and partial charge data for particular substructures, including amino acid side chains. The general form of the OPLS-AA force-field equation is described in eq 1. The term for the Urey−Bradley potential is not included because the OPLS-AA force field does not use it.

$$E_i^{\mathrm{MM}} = \sum_{\text{bonds}} K_r(r - r_0)^2 + \sum_{\text{angles}} K_\Theta(\Theta - \Theta_0)^2 + \sum_{\text{torsions}} \left(\frac{V_1^k}{2}[1 + \cos(\phi_i)] + \frac{V_2^k}{2}[1 + \cos(2\phi_i)] + \frac{V_3^k}{2}[1 + \cos(3\phi_i)] \right) + \sum_{k<l} \left(\frac{q_k q_l e^2}{r_{kl}} + 4\varepsilon_{kl}\left(\frac{\sigma_{kl}^{12}}{r_{kl}^{12}} - \frac{\sigma_{kl}^{6}}{r_{kl}^{6}} \right) \right) \quad (1)$$

The variables K_r and K_Θ are the stretching and bending force constants, whereas r_0 and Θ_0 are the bond length and bond angle parameters (reference bond length and reference bond angles), respectively. $(V_m^k)/2$'s are the torsional (out-of-plane) constants, while φ_k's are the corresponding proper or improper (out-of-plane) torsional angles. The q_k and q_l variables are the partial charges of the atoms, and r_{kl} is the distance between the interacting particles. ε_{kl} and σ_{kl} are the geometric mean values ($(\varepsilon_{kl} = (\varepsilon_k\varepsilon_l)^{1/2}$ and $\sigma_{kl} = (\sigma_k\sigma_l)^{1/2}$) of the atomic van der Waals parameters. The meaning of σ_{kl} and ε_{kl} in the Lennard-Jones type van der Waals term can be easily understood if we differentiate it with respect to the interatomic separation. It has a minimum (i.e., equilibrium interatomic separation) at $r_{kl} = \sigma_{kl}2^{1/6}$, and the value of the function (i.e., the Lennard-Jones type van der Waals energy) at this point is $-\varepsilon_{kl}$.

Glycyl radical parameters have already been developed for the OPLS-AA force field.[50] We will apply the same method as was used previously to develop parameters for the alanyl residue that will be compatible with the OPLS-AA force field.[49] These alanyl radical parameters will provide a more general parameter set that will be closer to those of the remaining amino acid with a C_β. These new parameters will enable the study of the structural consequences of C_α-centered radical in longer peptides and proteins and will be a suitable reference for the development of the remaining amino acid residues.

2. COMPUTATIONAL METHODS

2.1. Development of the Alanyl Radical Parameters.

Equation 1 can be used to compute the energy of a molecule in a particular geometry using the OPLS-AA force field, whereas the same structure can be computed with quantum chemical calculations using eq 2 to yield the E_i^{QM} energy, where $\hat{H}$ is the molecular Hamiltonian and Ψ is the wave function:

$$\hat{H}_i\psi = E_i^{\mathrm{QM}}\psi$$

The accuracy to which quantum mechanics can compute relative energy values (E_i^{QM}) for a series of selected geometries makes it an ideal choice for the development of molecular mechanical parameters. The fitting of the MM and QM data is accomplished by minimizing the molecular mechanics parameter-dependent sum of squares deviations between selected points of the two hypersurfaces. The approach corresponds to the simplified version of the general equation derived by Lifson and Warshel; however, the experimental values will be substituted with the quantum chemically derived ones.[35] This method has been explained in greater detail elsewhere.[35,39,40]

To derive the parameters, a series of computations were carried out for *N*-Ac-Ala$^{\bullet}$-*N*-methyl-amide, which is shown in Figure 1. The geometry of *N*-Ac-Ala$^{\bullet}$-*N*-methyl-amide was fully

optimized at the MP2/6-31+G(d,p) level of theory. Although a new atom type was defined for the carbon atom at the radical center (CRA), which is different from those at glycyl radical to allow more flexible parameter derivation, the van der Waals parameters were chosen to be identical for both of them. Therefore, the $\varepsilon = 0.066$ and $\sigma = 3.5$ Lennard-Jones parameters were used, which correspond to the C1/CT1 atom type of C_α atom. Because of the lack of reliable experimental heat of vaporization or heat of hydration data sets for α amino acid radicals, we derived the atomic charge parameters from restrained electrostatic potential (RESP) HF/6-31G(d) calculations.[51,52] The RESP method was originally recommended for AMBER force field; however, it was also used fruitfully for OPLS-AA force field in the case of missing charge parameters.[53,54] The RESP software can be downloaded from the AMBER Website.[55]

In principle, one can choose the geometries of the potential energy (hyper) surface at random when developing force field parameters, as it has been described elsewhere.[35,39,40] However, one has to keep in mind that each term of the empirical potential energy has its limitation. For example, the simple quadratic function for bond length and bond angle deformation in class I type force fields is an acceptable approximation for a quantum chemical potential energy curve only near to the corresponding equilibrium value. Similarly, for nonbonding terms at very short interatomic separation, a very large numerical difference can exist between the Lennard-Jones energy values and the quantum chemical ones. Therefore, only small perturbations from the equilibrium were allowed for the bond stretching and angle bending parameters, and the too short nonbonding interatomic separations were avoided.

Although the derivation of stretching parameters (because there is no linear dependence between them) is straightforward, the derivation of torsion and especially the bending parameters is somewhat more complicated. For the bending parameters, this is due to the fact that with new atom type at the vertex of a bond angle (where bond line segments meet) and with more than two bond lines with a common vertex, the bending parameters are not independents. Similarly, the torsion parameters are interdependent if the new (or newly parametrized) atom situated on the bond around which rotation parameters need to develop; that is, one of the two vertices of a three joining bond defines the dihedral angle.

To resolve the latter uncertainty, for example, in the case of the torsion around N−CRA bond (C−N−CRA−CT and H−N−CRA−CT torsions), only the $V_i^{\mathrm{C-N-CRA-CT}}$ torsion parameters were optimized (setting the $V_i^{\mathrm{C-N-CRA-CT}} = 0$ (i = 1,2,3)), then the $V_i^{\mathrm{C-N-CRA-CT}}$ values were distributed equally between $V_i^{\mathrm{C-N-CRA-CT}}$ and $V_i^{\mathrm{C-N-CRA-CT}}$ (i = 1,2,3). The N−CRA−C−O, N−CRA−C−N, C−N−CRA−C, H−N−CRA−C, CT1−C−N−CRA, O−C−N−CRA, H−N−C−CRA, and CT1−N−C−CRA torsion parameters were adopted from the glycyl radical force field.[50] Only the C−N−CRA−CT, H−N−CRA−CT, N−C−CRA−CT, O−C−CRA−CT, N−CRA−CT−H, and C−CRA−CT−H torsion parameters were developed. The rigid rotor approach was used to scan the torsion potential energy surface.

The development of bending parameters for the new CRA atom type (C−CRA−N, C−CRA−CT, and N−CRA−CT) was found to be more problematic due to the convergence problem caused by the interdependence of these parameters. Therefore, we used a grid-based method, which was combined with the least sum-of-square method mentioned above. We fixed the N−CRA−C parameters at $K_\Theta = 65.0$ kcal mol^{-1} rad^{-2} and $\Theta_0 = 118.0°$, and then in a range of 110.4°−130.4° and 110.7°−130.7° for the reference C−CRA−CT and N−CRA−CT angles, an equidistant 21 × 21 point grid was defined and the optimal (least-sum-of-squares deviation) K_Θ bending constants were obtained in one step at each grid point. We accepted those pairs of bending constants that are in the 50−75 kcal mol^{-1} rad^{-2} range and showed the least sum-of-squares deviation on this subset of grid points.

Similarly to the Gly C_α radical, the quantum chemical calculations for Ala C_α radical resulted in planar (or nearly planar) radical center with no chirality preferences. It can be assumed therefore that the improper torsion parameters along with the proper torsion ones in which the radical center involved give a satisfactory representation of the potential energy surface as was the situation at the glycyl radicals.[50] The out-of-plane motion of the glycyl radical has a very smooth character at small out-of-plane angle deviations (which corresponds to improper torsional angles near 0° or 180°), while its slope is much larger at angles far from the planarity. Substantially different improper torsion constant can be obtained, depending on the range of out-of-plane angle involved in parametrization process.[50] We intended to choose the golden mean; therefore, an MP2/6-31+G(d,p) energy scan of the out-of-plane angles between 0° and 45° was sampled more frequently at angles close to 0° in the parametrization. The out-of-plane angle is defined as the angle between the plane and the line segment defined by N−CRA−C atoms and the CRA−CT bond, respectively, as illustrated in Figure 2. It should be mentioned that this is not equal to the corresponding improper torsion angle.

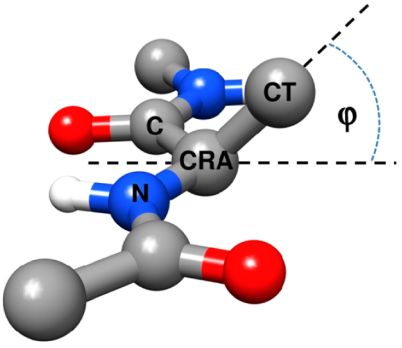

Figure 2. The out-of-plane angle, ϕ, used for geometry perturbation, which is however not equal to the improper torsion angle (angle between planes defined by C, N, CRA and N, CRA, CT atomic triples) for which the out-of-plane parameter was developed.

The proper torsion parameters were derived from LMP2/cc-pVTZ(-f) computations as was proposed by Kaminski et al. using the rigid rotor approach from the MP2/6-31+G(d,p) equilibrium geometry.[49] All other force field parameters were obtained with MP2/6-31+G(d,p) calculations. The points on the bond length, bond angle, and torsion angle potential energy curves and surfaces used to derive the parameters were generated systematically. The range of geometry variations and the points at which the energy calculations were carried out, relative to the MP2/6-31+G(d,p) equilibrium geometry, are shown in Table 1. Quantum chemical calculations were performed with the Gaussian 09, Gaussian 03, and Jaguar

Table 1. Variation in Bond Lengths, Bond Angles, and Torsional Angles Used To Parameterize the *N*-Ac-Ala$^{\bullet}$-Me Amide, Which Was Used To Represent the Ala Residue with a C_α Centered Radical[a]

parameter	atoms	variations
bond lengths	C−CRA CRA−CT CRA−N	±(0.001 Å, 0.002 Å, 0.003 Å, 0.005 Å, 0.008 Å, 0.011 Å, 0.016 Å, 0.021 Å, 0.026 Å, 0.031 Å, 0.036 Å, 0.041 Å)
bond angles	CRA−CT−H	±(0.1°, 0.2°, 0.3°, 0.4°, 1.0°, 1.5°, 2.0°, 2.5°, 3.0°, 3.5°, 4.0°, 5.0°, 6.0°, 7.0°, 8.0°)
	C−CRA−CT N−CRA−CT N−CRA−C	±n·0.1° (n = 0, 1, 2, ..., 25)
torsional angles	C−N−CRA−CT C−N−CRA−CT	30.0° increments for potential energy surface defined by C−N−CRA−CT and N−C−CRA−CT dihedral angle
	N−C−CRA−CT H−C−CRA−CT C−CRA−CT−H N−CRA−CT−H N−C−CRA−CT	15.0° increments for C−CRA−CT−H dihedral angle ±(1.0°, 2.0°, 5.0°, 7.0°, 10.0°, 12.0°, 15.0°, 20.0°, 25.0°, 30.0°, 35.0°, 40.0°, 45.0°) out-of-plane angle for N−C−CRA−CT improper torsion

[a]For bending parameters, the number of points on the hyper surface is $N = 2n_{max} + 1$.

software packages, while parameter fitting was carried out using a program developed in-house.[40,50,56−58]

2.2. Molecular Dynamics Simulations. *Simulation Conditions.* Using the newly developed alanyl radical parameters described in section 2.1, the conformational space of two heptapeptides was investigated with molecular dynamics simulations solvated with 2360 TIP4P water molecules in a cubic box of 41.7 Å × 41.7 Å × 41.7 Å.[59] The two model heptaalanyl peptides were used, *N*-Ac_1-Ala_2-Ala_3-Ala_4-Ala_5-Ala_6-Ala_7-Ala_8-Nma_9 (ALA) and *N*-Ac_1-Ala_2-Ala_3-Ala_4-Alr_5-Ala_6-Ala_7-Ala_8-Nma_9 (ALR), where the central alanine (Ala_5) of the latter peptide was modified manually into the radical form (Alr_5) by deleting the hydrogen from the C_α atom (Figure 3).

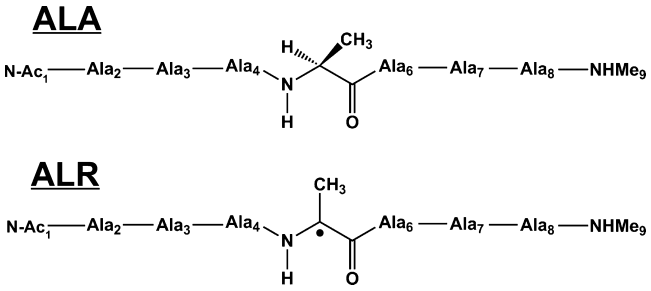

Figure 3. A schematic representation of the ALA and ALR heptapeptides. The ALR peptide contains the newly developed alanyl radical parameters.

The system was equilibrated with the provided protocol followed by a 96 ns simulation under NPT conditions (T = 310 K, P = 1.01325 bar) using the Martyna−Tobias−Klein pressure and temperature control.[60] A 2 fs integration step was used for the simulation, while the cutoff for the short-range nonbonded interactions was 9 Å and was updated every second step. Long-range electrostatic interactions were treated via the particle mesh Ewald method, containing 32 Fourier mesh points along each axis, and were updated every third integration step.[61] The structures were saved every 4.8 ps, which established a trajectory of 20 000 structures.

2.3. Molecular Dynamics Data Analysis. The density Ramachandran map was used to analyze the conformational space sampled by the Ala_5 or Alr_5 residues. The Ramachandran space was divided into 30° × 30° boxes, and the percentage of the structures in which Ala_5 or Alr_5 had ϕ and ψ angles values that fit within each box was reported. The number of secondary structure elements that were found in the discrete regions of the heptapeptides containing the Ala_5 or Alr_5 residues were quantified using secondary structure analysis (Table 2).

Table 2. Regions of the ALA and ALR Peptides Containing Residue Ala_5 or Alr_5, Which Were Used To Determine the Existence of Helical or Turn Structures[a]

peptide region	amino acid sequence	possible secondary structure
A2−A7	Ala_2-Ala_3-Ala_4-Xxx_5-Ala_6-Ala_7	π-turn or π-helix
A3−A8	Ala_3-Ala_4-Xxx_5-Ala_6-Ala_7-Ala_8	
A2−A6	Ala_2-Ala_3-Ala_4-Xxx_5-Ala_6	α-turn or α-helix
A3−A7	Ala_3-Ala_4-Xxx_5-Ala_6-Ala_7	
A4−A8	Ala_4-Xxx_5-Ala_6-Ala_7-Ala_8	
A2−A5	Ala_2-Ala_3-Ala_4-Xxx_5	β-turn or 3_{10}-helix
A3−A6	Ala_3-Ala_4-Xxx_5-Ala_6	
A4−A7	Ala_4-Xxx_5-Ala_6-Ala_7	
A5−A8	Xxx_5-Ala_6-Ala_7-Ala_8	
A3−A5	Ala_3-Ala_4-Xxx_5	γ-turn or inverse γ-turn
A4−A6	Ala_4-Xxx_5-Ala_6	
A5−A7	Xxx_5-Ala_6-Ala_7	
A4−A5	Ala_4-Xxx_5	δ-turn
A5−A6	Xxx_5-Ala_6	

[a]The Xxx_5 residue is the Ala_5 or Alr_5 residue.

The secondary structure elements consisted of individual β-, γ-, δ-, α-, and π-turns as described by Chou, and also higher-order secondary structure elements (SSE), which are composed of individual turns that combine to form helices.[62] The definition of the each secondary structure element can be found in Table 3, whereas Figure 4 contains a schematic diagram of the secondary structure elements.

Table 3. Definitions of the Secondary Structure Elements Used To Characterize the Structures of the ALA and ALR Peptides

secondary structure element	definition
Turn Structures	
δ-turn:	two consecutive residues with a hydrogen bond between NH_i and CO_{i+1}
γ-turn:	three consecutive residues with a hydrogen bond between CO_i and NH_{i+2}
inverse γ-turn:	three consecutive residues with a hydrogen bond between NH_i and CO_{i+2}
β-turn:	four consecutive residues with less than 7 Å between the C_α of residue "i" and residue "i + 3", in the absence of a helix
α-turn:	five consecutive residues with less than 7 Å between the C_α of residue "i" and residue "i + 4", in the absence of a helix
π-turn:	six consecutive residues with less than 7 Å between the C_α of residue "i" and residue "i + 5", in the absence of a helix
Higher-Order Structures	
3_{10}-helix:	two or more consecutive β-turns stabilized by hydrogen bonds
α-helix:	two or more consecutive α-turns stabilized by hydrogen bonds
π-helix:	two or more consecutive π-turns hydrogen bonds

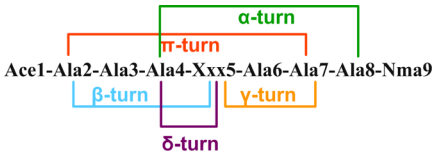

Figure 4. The possible secondary structure elements in the investigated peptides. The Xxx residue denotes Ala_5 or Alr_5 for the ALA and ALR heptapeptide, respectively.

A hydrogen bond was assigned to the peptide residues if the distance between the amide nitrogen and the carbonyl oxygen was less than 3.5 Å and the angle, α(N−H···O), was greater than 100°.

3. RESULTS

3.1. Parameterization Results. The atom centered partial charges derived from RESP calculations are shown in Figure 5.

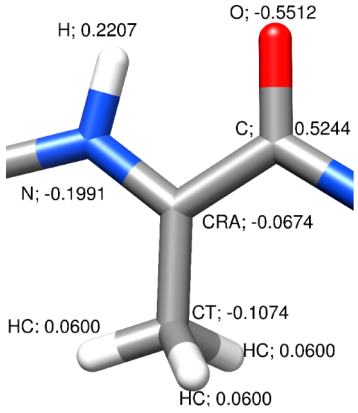

Figure 5. Atom types and partial charges for the alanyl α-radical (Alr_5) residue.

In Table 4, the newly developed stretching and bending parameters are listed together with the corresponding energy range spanned by the ab initio MP2/6-31+G(d,p) calculations, the number of points used for parametrization, and the sum of squares deviation between the two (hyper) surface measured at the geometries where the ab initio calculations were carried out. The parameters that were taken from the force field developed for the glycyl radical are also listed. As it was expected, excellent quality (regarding the sum of squares deviation) stretching parameters could be developed due to the fact that near the equilibrium the quadratic function is a good approximation for the bond length deformation.

When the new atom type belongs to only one of the two bonds constituting the bond angle, the force field angle parameters could be developed without any complication. This is demonstrated by the CRA−CT−H parameters, where the ab initio and optimized force-field surfaces fit remarkably well to each other. Contrarily, when the new atom type belongs to the common atom of more than one bond pair defining the bond angles to parametrize, the parameter development is more complicated. It was the case at parameter development for C−CRA−N, C−CRA−CT, and N−CRA−CT bond angles when we encountered convergence problems.

Therefore, the least sum-of-squares method was applied only for the bending constants development, and the optimal values for reference bond angles were found on a grid as was detailed in the Computational Methods. In this case, a much worse fit was obtained between QM and MM surfaces. Nevertheless, we used these parameters in OPLS-AA calculations.

Because we have already developed a set of parameters for the glycyl radical, it seemed to be reasonable to adopt those parameters for alanyl radical that belong to the same structural element of the radical center.[50] It can be presumed, for example, that the glycyl parameters for (H,O)−C−N−CRA and CRA−C−N−(H,CT) torsion can be used for alanyl radicals because they are related to peptide bond torsions. The only difference is in the origin of the otherwise highly similar CRA atom type (from either glycyl or alanyl residue). For the cases when the CRA atom participates in the central bond of a torsion, the glycyl parameters can be also adopted because the torsion parameters around the same bond are not independent and the occasional error introduced with the adopted parameters can be corrected with the newly developed parameters. It can be seen considering the fact that we a developed parameter set that with the already existing set gives in principle the "best" (least sum of squares of deviations) representation of the quantum chemical potential energy surface.

In other words, from a torsion point of view, the radical carbon atom type was the same for glycyl and alanyl radical, and new torsion constants were developed only for the new torsion type. For the CT−CRA−N−(H,C) and CT−CRA−C−(O,N) parameters, we followed the procedure that we

Table 4. Stretching and Bending Parameters Developed for Alanyl Radical, Energy Range Calculated during the MP2/6-31+G(d,p) Calculations, Number of Points (N) Used during Parameter Development, and Sum of Squares of Deviation (SSD, kcal mol^{-1}) between the Fitted Surfaces Measured at the Points Where the MP2/6-31+G(d,p) Calculations Were Carried Out

variable	atoms	parameters: bonds/kcal mol^{-1} Å^{-2}, angles/kcal mol^{-1} rad^{-2}	reference values: bonds/Å, angles/deg	energy range/kcal mol^{-1}	N	SSD
bonds	CRA−C	375.3	1.4547	0.9	75	0.004
	CRA−N	467.1	1.3643	0.9	75	
	CRA−CT	353.0	1.4760	0.9	75	
angles	CRA−N−C	43.59	119.12	adopted from glycyl radical force field[50]		
	CRA−N−H	24.96	122.42			
	CRA−C−O	65.04	123.94			
	CRA−C−N	68.75	118.14			
	CRA−CT−H	51.76	110.26	5.5	31	0.047
	C−CRA−N	65.00	118.00	0.5	153	
	C−CRA−CT	60.76	128.40	0.5	153	1.649
	N−CRA−CT	74.11	114.70	0.5	153	

Table 5. Proper and Improper Torsion Parameters (kcal mol^{-1}) Developed for Alanyl Radical, the Energy Range (kcal mol^{-1}) Spanned by LMP2/cc-pVTZ(-f) (MP2/6-31+G(d,p) for Out-of-Plane Parameters Calculations, the Number of Points (N) Used during Parameter Development, and the Sum of Squares Deviation (kcal mol^{-1})^2 between the Fitted Surfaces Measured at the Points Where the LMP2/cc-pVTZ(-f) (MP2/6-31+G(d,p) for Out-of-Plane) Calculations Were Carried Out[a]

	torsion parameters/kcal mol^{-1}					
variables	V_1	V_2	V_3	energy range/kcal mol^{-1}	N	SSD/kcal mol^{-1}
Proper Torsions						
CT1−C−N−CRA	−0.266	6.520	−0.544	values adopted from the glycyl radical force field[50]		
CT−C−N−CRA	−0.266	6.520	−0.544			
O−C−N−CRA	0.528	5.313	−0.822			
C−N−CRA−C	−2.939	4.402	−0.652			
H−N−CRA−C	2.939	4.402	0.652			
N−CRA−C−O	−0.279	1.911	−0.053			
N−CRA−C−N	0.279	1.911	0.053			
CRA−C−N−CT1	1.392	7.885	0.149			
CRA−C−N−CT	1.392	7.885	0.149			
CRA−C−N−H	0.0	5.949	0.0			
C−N−CRA−CT	2.079	3.691	1.064	20.0	104	190.284
H−N−CRA−CT	−2.079	3.691	−1.064	20.0	104	190.284
N−C−CRA−CT	0.476	2.363	0.014	20.0	104	190.284
O−C−CRA−CT	−0.476	2.363	−0.014	20.0	104	190.284
N−CRA−CT−HC	0.0	0.0	−1.431	1.0	25	13.350
C−CRA−CT−HC	0.0	0.0	1.431	1.0	25	13.350
Improper Torsions						
H−C−N−CRA	0.0	2.2	0.0	values adopted from the glycyl radical force field[50]		
CRA−N−C−O	0.0	21.0	0.0			
C−N−CRA−CT	0.0	3.391	0	9.8	25	0.210

[a] N = number of points on the hyper surface. SSD = sum of squares of deviation. For improper torsions, the third atom is the central one, and the first, second, and fourth atoms are connected to the third one. There is no chemical bond between the first, second, and fourth atoms.

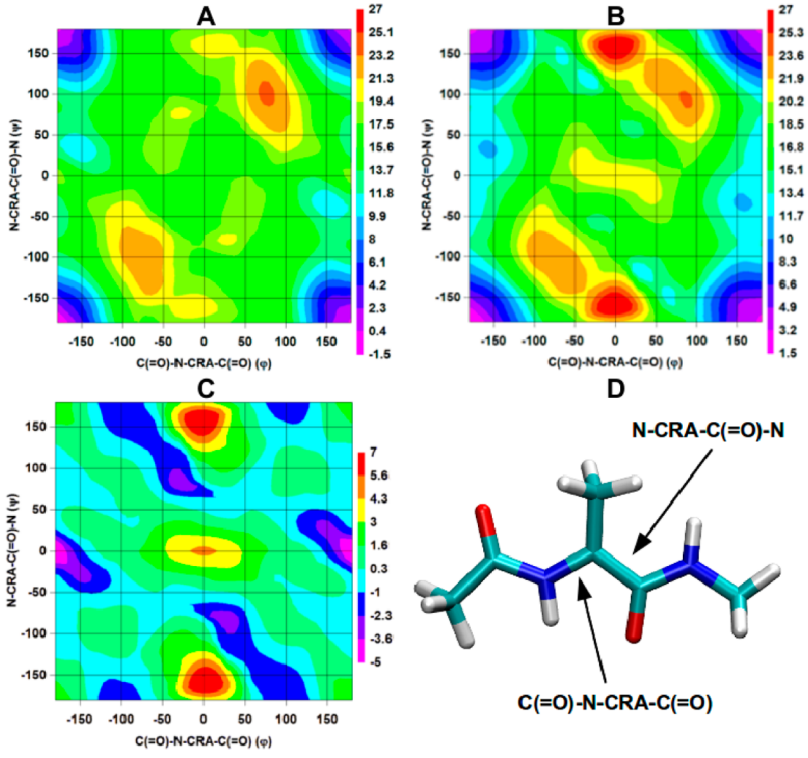

Figure 6. The LMP2/cc-pVTZ(-f) (A) and OPLS-AA (B) potential energy surfaces for Ac-Ala-NHMe as a function of C′(═O)−N−CRA−C(═O) and N−CRA−C(═O)−N′ torsion angles and their difference map (C). The torsional angles are illustrated in panel D. For the crude maps, only those points were considered where the relative energy (as compared to the global torsion minimum) did not exceed the 20.0 kcal mol^{-1} cutoff value. The maps were then smoothed by interpolation. The regions that did not meet the 20 kcal mol^{-1} cutoff criterion were completed by extrapolation.

dx.doi.org/10.1021/ct300059f | J. Chem. Theory Comput. 2012, 8, 2569−2580

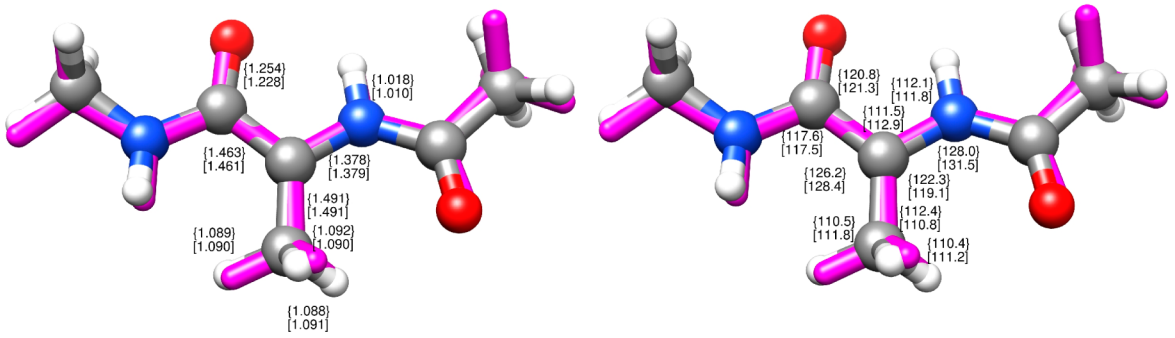

Figure 7. Superposed *N*-Ac-Ala$^{\bullet}$-NHMe structures calculated at MP2/6-31+G(d,p) (ball and stick) and the same structure computed with the newly developed OPLS-AA force field (stick only). The bond lengths, in angstroms, are shown in the left panel, whereas the bond angles (in deg) are shown in the right panel. MP2/6-31+G(d,p) and OPLS-AA force-field geometry parameters are in braces and brackets, respectively.

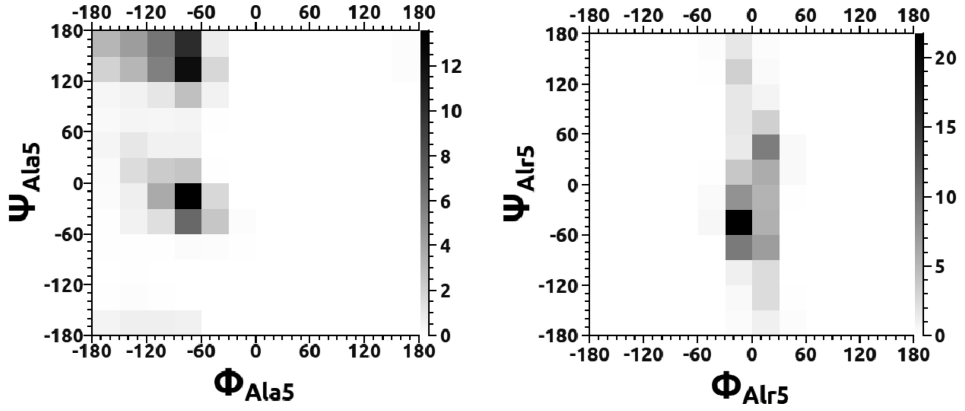

Figure 8. The density Ramachandran maps of the central amino acid (Ala5 or Alr5) for the ALA (left) and ALR (right) peptides.

applied at glycyl radical parametrization, and the two-dimensional (Ramachandran-like φ,ψ) torsion energy surface was generated and the torsion parameters were simultaneously fitted.[50] The new proper torsion parameters along with the adopted ones are listed in Table 5.

Because the repulsive van der Waals term is only an approximation to the repulsion between interacting atoms in a molecule, and because the van der Waals energy changes rapidly at shorter distances, the contribution of this energy term to the total energy affected with greater error at nearby atoms. Therefore, only those points on the surface were considered in parametrization, which has smaller relative energy (as compared to the global minimum) than the 20.0 kcal mol^{-1} cutoff.

In Figure 6, the φ,ψ torsion potential energy map from quantum chemical calculations (Figure 6A) and from OPLS-AA empirical force field calculations using the newly developed parameters (Figure 6B) is shown together with the difference map of them (Figure 6C). It is immediately apparent from Figure 6A and B that the global energy minimum is around the ±180° CT−CRA−N−(H,C) and ±180° CT−CRA−C−(O,N) dihedral angles. These points (which certainly only one point on the potential energy surface) correspond to the nearly coplanar peptide bond arrangement.

Regarding the energy difference between the LMP2/cc-pVTZ(-f) and the OPLS-AA energy surfaces shown in Figure 6C, apart from a few localized regions, a nice overall agreement (with deviation within a −1.0 and 3.0 kcal/mol range) can be seen between the ab initio and force field surfaces. The empirical force field overestimates the energies in the regions at ψ = ∼180° and ψ = ∼0° when φ = ∼0°, whereas it underestimates the energies near the 180°/0°, 30°/−80°, and 100°/180° φ/ψ torsion angle pairs.

The N−CRA−CT−HC and C−CRA−CT−HC parameters also had to be developed. As it can be seen from Table 5, these parameters can be featured by a pure V_3 term, which is usual for this kind of torsion. Accepting the sum of squares deviation as a quantitative characterization of parameter fitting, the conclusion can be drawn that the rotation energy profile is poorly represented by the truncated trigonometric series applied in the OPLS-AA force field. It should be mentioned that we tried separate V_1, V_2, and V_3 terms and all of their combinations, but we either encountered convergence problem or got even worse fitting. The reason can be the imperfect representation of nonbonded interaction in OPLS-AA; for example, the amide proton does not contribute to the van der Waals interaction, while it contributes to electrostatic interaction. Notwithstanding, we used these parameters in the OPLS-AA calculations.

The value obtained for the out-of-plane improper torsion parameter is listed also in Table 5. Despite the relatively large out-of-plane motion, the parameter obtained for the corresponding improper torsion almost perfectly describes the out-of-plane energy profile, and the sum of squares deviation at these points is only 0.210 (kcal mol^{-1})^2, while the energy range we used for parameter fitting was ∼10 kcal mol^{-1}. The minimum energy structures obtained from MP2/6-31+G(d,p) and OPLS-AA calculations were superposed to check the quality of the new OPLS-AA alanyl radical parameters. It is immediately apparent that they fit to each other almost perfectly, especially at the radical center region (Figure 7).

dx.doi.org/10.1021/ct300059f | J. Chem. Theory Comput. 2012, 8, 2569−2580

Regarding the numerical values, noticeably differences between MP2 and OPLS-AA bond length can be found only at the C=O bond. It should be mentioned, however, that for this bond the original OPLS-AA peptide carbonyl parameters were used in which the more extended conjugation through the nearly planar radical (as compared to isolated peptide bond fragment) was not considered. The equilibrium ab initio and force field bond angle values demonstrate noteworthy agreement as well. The deviations are dominantly less than 2°. The maximum deviation is 3.5° for CRA−N−C angle; however, for this angle, the parameter was adopted from the glycyl radical force field.[50]

3.2. Molecular Dynamics Simulations. *Geometry of the Central Residue (Ala_5 or Alr_5) of the Heptapeptides.* The density Ramachandran map (Figure 8) indicates that the most populated region of the Ramachandran space of Ala_5 was when ϕ was between −90° and −60° and when ψ was between −30° and 0°, which contained 13.6% of the structures. The highest populated region occupying Alr_5 was when ϕ was between −30° and 0° and when ψ was between −60° and −30°, which includes 21.7% of the structures. Moreover, the Ramachandran map of Alr_5 shows that the region where ϕ is between −30° and 30° was also highly populated.

The distribution of the distance between the carbonyl oxygen of Ala3, Ala4, and Ala5 (residue "i") of ALA and the amide hydrogen of its corresponding "i + 2" residue, Ala5, Ala6, and Ala7, respectively, was plotted to determine if hydrogen bonds between these residue pairs can enable γ-turn formation. The same residue pairs were plotted for the ALR peptide (Figure 9).

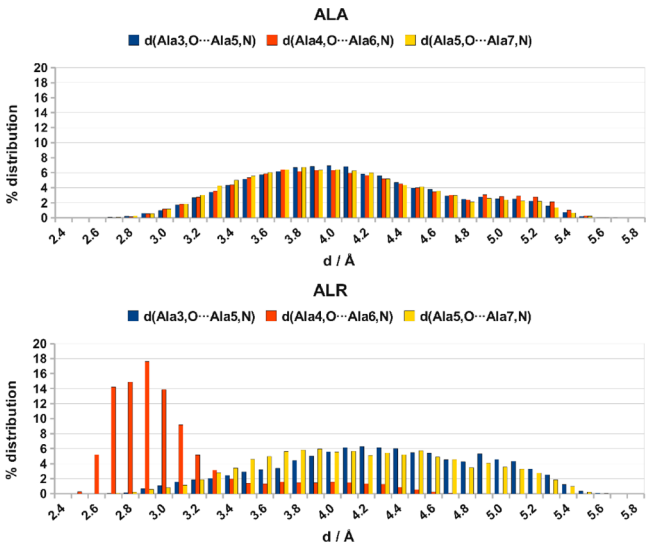

Figure 9. The distribution of the structures according to the distance between the carbonyl oxygen and amide nitrogen of residues Ala_3 and Ala_5, those of Ala_4 and Ala_6, and those of Ala_5 and Ala_7.

A similar distribution of the interatomic distances was shown for ALA and ALR when Ala_5 or Alr_5 was at the first or third residue of the "i" or at the residue "i + 2" position. These values were most frequently between 3.8 and 4.1 Å in ALA, and between 4.1 and 4.4 Å in ALR. However, this distance is reduced to approximately 2.95 Å in ALR when Alr_5 is the central residue "i + 1" of the turn. This distance shortening increased the propensity of hydrogen bonds to form between the atom pairs and enabled γ-turns to form in this region of the peptide.

Analysis of the Secondary Structure Elements. Analysis of the secondary structure elements showed that only γ-, β-, α-, and π-turn structures were observed in the ALA and ALR peptides, whereas neither δ- nor inverse γ-turns were detected. These results are shown in Table 6.

Table 6. Number of Turn Structures Identified in the ALA and ALR Heptapeptides[a]

	heptapeptide			heptapeptide	
secondary structure element	ALA	ALR	secondary structure element	ALA	ALR
γ-turn (i = 3)	1781	1273	α-turn (i = 2)	1549	2794
γ-turn (i = 4)	1493	7936	α-turn (Hb, i = 2)	1375	25
γ-turn (i = 5)	2107	1366	α-turn (i = 2)	2212	8829
β-turn (i = 2)	3858	1730	α-turn (Hb, i = 3)	926	29
β-turn (Hb, i = 2)	1953	15	α-turn (i = 4)	1859	3020
β-turn (i = 3)	3356	2292	α-turn (Hb, i = 4)	1015	2510
β-turn (Hb, i = 3)	1693	228	π-turn (i = 2)	1266	3645
β-turn (i = 4)	3323	1457	π-turn (Hb, i = 2)	135	44
β-turn (Hb, i = 4)	2277	8371	π-turn (i = 3)	1626	8050
β-turn (i = 5)	3874	4519	π-turn (Hb, i = 3)	1	26
β-turn (Hb, i = 5)	1661	1074			

[a]The residue that starts the turn is residue "i", whereas Hb denotes the turn structures that were stabilized by hydrogen bonds.

More than 4 times more γ-turns (i = 4), β-turns (Hb, i = 4), α-turns (i = 2), and π-turns (i = 3) were observed in ALR than were observed in ALA. The largest difference in the number of turn structures was observed in the γ-turn (i = 4) structures, which showed a 5.3-fold increase in frequency in ALR than in ALA.

Higher-Order Secondary Structure Elements. Of the 20 000 structures sampled, only 1578 and 1043 helices were observed in ALA and ALR, respectively (Table 7). 3_{10}-helices of various lengths were observed in the ALA peptide, where seven structures were identified that contained all seven residues in a 3_{10}-helix. Shorter helices were identified more frequently, and a relatively equal number of shorter helices were observed at the N and C termini. The ALR only contained short 3_{10}-helices, and 1037 of 1038 of the helices involved residues A4−A8. The α-helix was observed in 670 ALA structures, and 163 of those structures involved residues A2−A8. Shorter helices were also identified with a higher frequency than the longer ones, and they were identified at a higher frequency at the N-terminus

Table 7. Number of Higher-Ordered Structures Observed in the Defined Regions of the ALA and ALR Peptides[a]

		heptapeptide	
higher-ordered structure	peptide region	ALA	ALR
3_{10}-helix	A2−A8	7	
	A2−A7	52	
	A3−A8	40	
	A2−A6	287	1
	A3−A7	172	
	A4−A8	350	1037
α-helix	A2−A8	163	
	A2−A7	305	
	A3−A8	202	
π-helix	A2−A8	0	5

[a]The peptide regions are defined in Table 2.

dx.doi.org/10.1021/ct300059f | J. Chem. Theory Comput. 2012, 8, 2569−2580

than at the C-terminus. No α-helices were observed in the ALR peptide, and π-helices were only observed five times in the ALR peptide. Representative structures of ALR are shown in Figure 10.

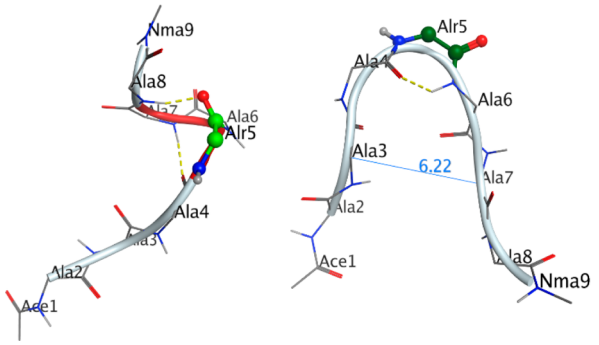

Figure 10. Representative 3_{10} helix (left) and α-turn (right) structures of the ALR peptide. The helix contains hydrogen bonds between the C═O of Ala_4 and N−H of Ala_7 (2.98 Å, 172.7°) and those of Ala_5 and Ala_8, respectively (2.70 Å, 164.2°). The turn contains a hydrogen bond between the C═O of Ala_4 and N−H of Ala_6 (2.72 Å, 129.0°). The Alr_5 residue is shown in the CPK representation.

The π-turn structures occurred more frequently in ALR than in ALA, with at least 3 times more π-turns structures observed at each position of ALR than were observed in the respective position of ALA. The largest difference was observed in the A3−A8 region, where almost 5 times more π-turns were observed in ALR than in ALA (Table 8).

The frequency of the total number of α-turn structures observed in ALA and ALR was more similar; however, a 3-fold increase in the number of α-turns was observed in the A3−A7 region in ALR as compared to in ALA. In this region, the Alr_5 residue is in the central position of the turn. The Alr_5 residue also formed more γ-turns, which involves three residues, when it was in the central position of the turn than did the Ala_5 residue (Table 6). The propensity of Alr_5 to form a γ-turn was less than that of the Ala_5 when the first and third positions are compared. In the case of the β-turns with hydrogen bonds, which involves four residues, the Alr_5 residue formed 5 times more β-turns when it was in the second position of the turn. Hydrogen-bonded β-turns, which contained the Alr_5 in position three of the β-turn, were less numerous than when Ala_5 was in this position.

4. DISCUSSION

4.1. Force-Field Parameterization. Comparing the reference bond length and angle (Table 4) values to the corresponding MP2/6-31+G(d,p) equilibrium values (Figure 7), it can be seen that noticeable differences exist between them. For example, the CRA−CT equilibrium bond distance is 1.491 Å at MP2/6-31+G(d,p) level, while its reference value for OPLS-AA force field we obtained from such calculations is 1.476 Å. Using this latter reference bond length in the OPLS-AA calculation, we can reproduce almost perfectly the MP2/6-31+G(d,p) value. It underlines the importance that the interaction can influence the equilibrium bond length at empirical force-field level during parametrization. It also draws our attention that using quantum chemical equilibrium values as empirical force field reference values should be avoided whenever possible. Similar and even more remarkable facts can be observed comparing the ab initio MP2/6-31+G(d,p) equilibrium and the corresponding reference bond angle values obtained from parametrization.

Table 8. Distribution of the Turn Structures (Isolated and Consecutive) among the Various Regions for ALA and ALR[a]

peptide region				number of turns	
A2−A7	A3−A8			ALA	ALR
π-turn	π-turn			264	1270
π-turn	Ø			846	2270
Ø	π-turn			1264	5866
A2−A6	A3−A7	A4−A8		ALA	ALR
α-turn	α-turn	α-turn		144	1
α-turn	α-turn	Ø		337	1
Ø	α-turn	α-turn		66	97
α-turn	Ø	α-turn		36	0
α-turn	Ø	Ø		817	748
Ø	α-turn	Ø		411	1266
Ø	Ø	α-turn		807	117
A2−A5	A3−A6	A4−A7	A5−A8	ALA	ALR
β-turn	β-turn	β-turn	β-turn	22	0
β-turn	β-turn	β-turn	Ø	94	0
Ø	β-turn	β-turn	β-turn	25	0
β-turn	β-turn	Ø	β-turn	22	0
β-turn	Ø	β-turn	β-turn	18	2
β-turn	β-turn	Ø	Ø	257	4
Ø	β-turn	β-turn	Ø	59	0
Ø	Ø	β-turn	β-turn	131	39
β-turn	Ø	β-turn	Ø	206	37
β-turn	Ø	Ø	β-turn	282	3
Ø	β-turn	Ø	β-turn	110	95
β-turn	Ø	Ø	Ø	1676	88
Ø	β-turn	Ø	Ø	991	1179
Ø	Ø	β-turn	Ø	954	430
Ø	Ø	Ø	β-turn	1501	121
A3−A5	A4−A6	A5−A7		ALA	ALR
γ-turn	γ-turn	γ-turn		0	10
	Ø			21	176
Ø	γ-turn	γ-turn		18	121
γ-turn	Ø	γ-turn		35	10
γ-turn	Ø	Ø		473	191
Ø	γ-turn	Ø		285	1624
Ø	Ø	γ-turn		395	180

[a]The Ø symbol indicates the absence of a turn. The peptide regions are defined in Table 2.

Regarding the torsion parameters, in addition to the global energy minimum at 180°/180° φ,ψ angle pair, further local energy minima also can be found on both the LMP2/cc-pVTZ(-f) and the OPLS-AA surfaces (e.g., around the −150° and 40° φ,ψ pair). The high energy regions of these surface can be found at the vicinity of 0° and 180° as well as 90° and 90° φ,ψ angle pairs. On the LMP2/cc-pVTZ(-f) potential energy surface, another high energy region also can be found in the neighborhood of −30°/80° φ/ψ torsion angles. Because of the planar heavy atom geometry and the rigid rotor approach we used to generate the rotation energy surface, the corresponding symmetry related image of these points also exists on the surface.

The largest positive deviations between the quantum mechanical (LMP2/cc-pVTZ(-f)) and OPLS-AA empirical force field (using the parameters developed in this work) energy surfaces shown in Figure 6 can be explained by the

overestimated nonbonded (van der Waals and electrostatic) repulsion at the corresponding regions (e.g., at 0°/180° φ,ψ torsion angles). Contrarily, the largest negative one is the omitted van der Waals interaction for amide H in OPLS-AA force field, which results in an underestimated relative energy near the 180°/0° φ,ψ torsion angle pair, where the two amide protons are close to each other but there is no van der Waals interaction between them.

The C−N−CRA−CT improper torsion parameter was found to be larger than the peptide amide parameter but smaller than the peptide carbonyl parameter. It was larger than the improper (torsion) term obtained for glycyl radical; partially because of the larger amplitude motion (within ±45° out-of-plane angle), we intended to yield reasonable out-of-plane energies. The value obtained for the out-of-plane improper torsion parameter was certainly not independent from newly developed torsion parameters. It is necessary to account for the torsional contribution to the out-of-plane energy during parameter development, which is done automatically in our software.

4.2. Molecular Dynamics Simulations. The highly populated regions of the Ala_5 and Alr_5 Ramachandran maps, shown in Figure 8, clearly indicate the effect of the new parameters on the conformations of the Alr_5 residue. The Ala_5 maps show that the ϕ and ψ angles of the central residue of the pentapeptide are in agreement with the ϕ and ψ angles of L-amino acid residues.[63] The ϕ and ψ angles of the central residue of the Alr peptide are much different. It has been shown previously that the ϕ and ψ angles that correspond to "planar" conformations (with ϕ and ψ torsions near 0° or 180°) are the most stable in residues that contain a C_α-centered radical.[25] This phenomenon has now been demonstrated in the alanyl radical parameters developed herein; however, the planarity is more prominent in the ϕ (C−N−CRA−C) torsion than in the ψ (N−CRA−C−N) torsion. This is in agreement with experiments, which have shown that C_α-centered radical center in peptides have a stronger coupling to the amide nitrogen then to the carbonyl carbon.[22,64] The global minimum of the *N*-Ac-Ala$^\bullet$-NHMe potential energy surface can be found within the β_L conformational space; however, this may be a property of the monoamino acid model that was used in that particular case. The planar conformers that enable the heptapeptide to form a γ-turn were populated more frequently when alanyl radical parameters were used. This can be due to the stabilization from intramolecular hydrogen bonds, but can also be a function of peptide length and the type of water molecules. These parameters provide the means for these effects to be studied in the future.

The difference between the frequency of which the various β-turn structures were formed in ALA and ALR suggests that Alr_5 in position two of the β-turn stabilizes hydrogen bonds, whereas Alr_5 in position three of the turn destabilizes hydrogen bonds. When the turn-forming propensityies of the three central residues of the α-helices are compared, more α-turns were formed when Alr_5 was present than for Ala_5; however, the difference was the greatest when Alr_5 was in the central position of the α-turn. Two of the six residues of the π-turn can be considered as central, and the Alr_5 residue formed more turns than Ala_5 in both of these positions, with more turns forming when Alr_5 was in the second of the two central residues.

The increased propensity of Alr_5 to form a turn when in the C-terminal central position of the β-turn and π-turn could be due to the confinement of the ϕ dihedral angle of Alr_5 to values close to 0°, as shown in Figure 10, which stabilized the turn. The ψ dihedral showed more variations in its angle; therefore, less turns were stabilized in the N-terminal central position.

Sequential and overlapping regions of turns and helices are the building blocks of higher-order structures. Table 8 contains the number of higher-order turn structures. The ability of the Alr_5 residue to form γ-turns in the middle residue of the turn is the main reason why higher order γ-turn structures are more prevalent because a γ-turn consists of only three residues. There are no cases in which higher-order β-turn and α-turn structures are more prevalent in the ALA peptide than in the ALR peptide. An isolated β-turn from Ala_3 to Ala_6 and an isolated α-turn from A3 to A7, both of which contain Alr_5 in position three of the respective turn, are the only turn motifs that are more numerous in ALR than in ALA. The overlapping A2−A7 and A3−A8 π-turn regions are more numerous in ALR than in ALA, which can be attributed to the increased number of the individual π-turns containing the Alr_5 residue.

Helices were not highly prevalent in either the ALA or the ALR peptide, as shown in Table 7. The ALR peptide did not contain multiple overlapping helical structures, with the exception of the 3_{10} helices in the overlapping A4−A7 and A5−A8 regions. In this region, the Alr_5 structure occupied one of the two central positions of the helices. The Alr_5 residue did not form a single α-helix. This suggests that the ideal ϕ and ψ angles of the Alr_5 residue are not conducive to α-helix formation, especially considering this structure is observed in the ALA peptide and also in the longer π-helix. Molecular simulations of longer duration and using longer Alr-containing peptides will enable this assumption to be made with greater certainty.

The Alr_5 residue stabilizes turns or helices only when it occupies a central position of a turn or a helix; however, the Alr_5 residue destabilizes higher-ordered structures that are made from β-turns and α-turns. This suggests that the use of the alanyl radical residue parameters will destabilize secondary structure elements greater than six residues in length and will likely increase the disorder in a peptide and contribute to the unfolding of a protein. The formation of an individual turn or helix could provide the nucleation point in structures containing peptide aggregates. Further investigation of peptides, proteins, and their aggregates, which include the alanyl radical parameters, will help to validate these hypotheses.

5. CONCLUSIONS

Comparing the quantum chemical equilibrium bond length and bond angle values to the "reference" bond lengths and angles derived for the OPLS-AA force field by means of these QM calculations clearly indicates that the equilibrium QM lengths and angles should not be used as a "reference" r_0 and Θ_0. The rigid-rotor approach used to obtain the torsional parameters showed a good agreement between the LMP2/cc-pVTZ(-f) and OPLS-AA torsional potential energy surfaces. The slight difference between these two surfaces can be attributed to the overestimation of the electrostatic and van der Waals interaction energies. Moreover, the interdependence of the out-of-plane (improper) torsional and the proper torsional energies underlines the importance of considering all of the already existing parameters during parameter development. In other words, new parameters should be always developed taking into account all energy terms in the particular force field equation.

The new parameters were incorporated into the Alr5 residue to enable the secondary structures of the ALR peptide to be compared to those of the closed-shell, ALA peptide. The ALR peptide formed more γ-turns and α-turns than the ALA peptide when the Alr_5 residue occupied the central position of the turn. When there were two central positions, as there are in β-turns and π-turns, the ALR peptide contained more such turns than the ALA peptide when the Alr_5 residue was in the second position of the central turn residues. The stability of higher-order structures consisting of γ-turns and π-turns increased when Alr_5 is present, whereas the stability of higher-order structures made from β-turns and α-turns decreased when Alr_5 is present. Because of the general destabilization of higher-ordered structures, the use of the alanyl radical parameters should increase the disorder of peptides and contribute to the unfolding of proteins.

■ ASSOCIATED CONTENT

Supporting Information

Pre-equilibration protocol for the molecular dynamics simulations. This material is available free of charge via the Internet at http://pubs.acs.org.

■ AUTHOR INFORMATION

Corresponding Author

*Phone: (36-62) 544720. Fax: (36-62) 420953. E-mail: viskolcz@jgypk.u-szeged.hu.

Notes

The authors declare no competing financial interest.

■ ACKNOWLEDGMENTS

We thank László Müller and Máté Labádi for the administration of the computing systems used for this work. This work was supported by the project TAMOP-4.2.1/B-09/1/KONV-2010-0005-Creating the Center of Excellence at the University of Szeged, which is supported by the European Union and cofinanced by the European Regional Fund. This work was supported by the Faculty Grant CS-007/2010 and the Hungarian National Infrastructure Development Program (Grant NIIF 1057).

■ REFERENCES

(1) Davies, K. J. A.; Delsignore, M. E.; Lin, S. W. *J. Biol. Chem.* **1987**, *262*, 9902−9907.
(2) Davies, K. J. A. *J. Biol. Chem.* **1987**, *262*, 9895−9901.
(3) Barnham, K. J.; Masters, C. L.; Bush, A. I. *Nat. Rev. Drug Discovery* **2004**, *3*, 205−214.
(4) Kobliashev, V. A. *Biochemistry (Moscow)* **2010**, *75*, 675−685.
(5) Fatehi-Hassanabad, Z.; Chan, C. B.; Furman, B. L. *Eur. J. Pharmacol.* **2010**, *636*, 8−17.
(6) Spiteller, G. *Free Radical Biol. Med.* **2006**, *41*, 362−387.
(7) Grimm, S.; Hoehn, A; Davies, K. J.; Grune, T. *Free Radical Res.* **2011**, *45*, 73−88.
(8) Hardy, J. A.; Higgins, G. A. ???? **1992**, *256*, 184−185.
(9) Funke, S. A. *Int. J. Alzheimer's Dis.* **2011**, ID: 151645.
(10) Mao, X.; Wang, C.; Wu, X.; Ma, X.; Liu, L.; Zhang, L.; Niu, L.; Guo, Y.; Li, D.; Yang, Y.; Wang, C. *Proc. Natl. Acad. Sci. U.S.A.* **2011**, 1102971108.
(11) Perczel, A.; Hudáky, P.; Pálfi, V. K. *J. Am. Chem. Soc.* **2007**, *129*, 14959−14965.
(12) Owen, M. C.; Viskolcz, B.; Csizmadia, I. G. *J. Phys. Chem. B* **2011**, *115*, 8014−8023.
(13) Owen, M. C.; Viskolcz, B.; Csizmadia, I. G. *J. Chem. Phys.* **2011**, *135*, 035101.
(14) Rauk, A.; Yu, D.; Armstrong, D. A. *J. Am. Chem. Soc.* **1997**, *119*, 208−217.
(15) Armstrong, D. A.; Yu, D.; Rauk, A. *Can. J. Chem.* **1996**, *74*, 1192−1199.
(16) Rauk, A.; Yu, D.; Taylor, J.; Shustov, G.; Block, D.; Armstrong, D. *Biochemistry* **1999**, *39*, 9089−9096.
(17) Galano, A.; Alvarez-Idaboy, J. R.; Montero, L. A.; Vivier-Bunge, A. *J. Comput. Chem.* **2001**, *22*, 1138−1153.
(18) Galano, A.; Alvarez-Idaboy, J. R.; Bravo-Pérez, G.; Ruiz-Santoyo, M. E. *J. Mol. Struct. (THEOCHEM)* **2002**, *617*, 77−86.
(19) Huang, M. L.; Rauk, A. *J. Phys. Org. Chem.* **2004**, *17*, 777−786.
(20) Zhu, R.; Lin, M. *J. Phys. Chem. A* **2001**, *105*, 6243−6248.
(21) Chersakov, A.; Jonsson, M. *J. Chem. Inf. Comput. Sci.* **2000**, *40*, 1222−1226.
(22) MacInnes, I.; Walton, J. C.; Nonhebel, D. C. *J. Chem. Soc., Chem. Commun.* **1985**, 712−713.
(23) Viehe, H.-G.; Janousek, Z.; Mirnyi, R.; Stella, L. *Acc. Chem. Res.* **1985**, *18*, 148−154.
(24) Garrison, W. M. *Chem. Rev.* **1987**, *87*, 381−398.
(25) Owen, M. C.; Szöri, M.; Csizmadia, I. G.; Viskolcz, B. *J. Phys. Chem. B* **2012**, *116*, 1143−1154.
(26) Weiner, P. K.; Kollman, P. A. *J. Comput. Chem.* **1981**, *2*, 287−303.
(27) Brooks, B. R.; Bruccoleri, R. E.; Olafson, B. D.; States, D. J.; Swaminathan, S.; Karplus, M. *J. Comput. Chem.* **1983**, *4*, 187−217.
(28) Jorgensen, W. L.; Maxwell, D. S.; Tirado-Rives, J. *J. Am. Chem. Soc.* **1996**, *118*, 11225−11236.
(29) Unkrig, V.; Neugebauer, F. A.; Knappe, J. *Eur. J. Biochem.* **1989**, *184*, 723−728.
(30) Parast, C. V.; Wong, K. K.; Lewisch, S. A.; Kozarich, J. W. *Biochemistry* **1995**, *34*, 2393−2399.
(31) Mulliez, E.; Fontecave, M.; Gaillard, J.; Reichard, P. *J. Biol. Chem.* **1993**, *268*, 2296−2299.
(32) Stadtman, E. R. *Science* **1992**, *257*, 1220−1224.
(33) Perez-Campo, R.; López-Torres, M.; Cadenas, S.; Rojas, C.; Barja, G. *J. Comp. Physiol., B* **1998**, *168*, 149−158.
(34) Brunelle, P.; Rauk, A. *J. Alzheimer's Dis.* **2002**, *4*, 283−289.
(35) Lifson, S.; Warshel, A. *J. Chem. Phys.* **1968**, *49*, 5116−5129.
(36) Hagler, A. T.; Huler, E.; Lifson, S. *J. Am. Chem. Soc.* **1974**, *96*, 5319−5327.
(37) Hagler, A. T.; Lifson, S. *J. Am. Chem. Soc.* **1974**, *96*, 5327−5335.
(38) Maple, J. R.; Dinur, U.; Hagler, A. T. *Proc. Natl. Acad. Sci. U.S.A.* **1988**, *85*, 5350−5354.
(39) Tronchet, J. M. J.; Komáromi, I. *Int. J. Biol. Macromol.* **1993**, *15*, 69−72.
(40) Komáromi, I.; Tronchet, J. M. J. *J. Mol. Struct. (THEOCHEM)* **1997**, *395*, 15−28.
(41) Ferré, N.; Cembran, A.; Garavelli, M.; Olivucci, M. *Theor. Chem. Acc.* **2004**, *112*, 335−341.
(42) Carbonnaire, P.; Begue, D.; Dargelos, A.; Pouchan, C. *Chem. Phys.* **2004**, *300*, 41−51.
(43) MacKerell, A. D., Jr.; Bashford, D.; Bellott, M.; Dunbrack, R. L., Jr.; Evanseck, J. D.; Field, M. J.; Fischer, S.; Gao, J.; Guo, H.; Ha, S.; Joseph-McCarthy, D.; Kuchnir, L.; Kuczera, K.; Lau, F. T. K.; Mattos, C.; Michnick, S.; Ngo, T.; Nguyen, D. T.; Prodhom, B.; Reiher, W. E., III; Roux, B.; Schlenkrich, M.; Smith, J. C.; Stote, R.; Straub, J.; Watanabe, M.; Wiórkiewicz-Kuczera, J.; Yin, D.; Karplus, M. *J. Phys. Chem. B* **1998**, *102*, 3586−3616.
(44) Foloppe, N.; MacKerell, A. D., Jr. *J. Comput. Chem.* **2000**, *21*, 86−104.
(45) Barone, V.; Capecchi, G.; Brunel, Y.; Dheu, M. -L.; Subra, R. *J. Comput. Chem.* **1997**, *18*, 1720−1728.
(46) Leach, A. L. *Molecular Modelling: Principles and Applications*, 2nd ed.; Prentice Hall: New York, 2001.
(47) Hwang, M. J.; Stockfish, T. P.; Hagler, A. T. *J. Am. Chem. Soc.* **1994**, *116*, 2515−2525.
(48) Maxwell, D. S.; Tirado-Rives, J.; Jorgensen, W. L. *J. Comput. Chem.* **1995**, *16*, 984−1010.

(49) Kaminski, G.; Friesner, R. A.; Tirado-Rives, J.; Jorgensen, W. L. *J. Phys. Chem. B* **2001**, *105*, 6474−6487.
(50) Komáromi, I.; Owen, M. C.; Murphy, R. F.; Lovas, S. *J. Comput. Chem.* **2008**, *29*, 1999−2009.
(51) Bayly, C. I.; Cieplak, P.; Cornell, W. D.; Kollman, P. A. *J. Phys. Chem.* **1993**, *97*, 10269−10280.
(52) Cornell, W. D.; Cieplak, P.; Bayly, C. I.; Gould, I. R.; Merz, K. M.; Ferguson, D. M.; Spellmeyer, D. C.; Fox, T.; Caldwell, J. W.; Kollman, P. A. *J. Am. Chem. Soc.* **1995**, *117*, 5179−5197.
(53) Kahn, K.; Bruice, T. C. *J. Comput. Chem.* **2002**, *23*, 977−996.
(54) Beckstein, O.; Iorga, B. I. *J. Comput.-Aided Mol. Des.* **2012**, DOI: 10.1007/s10822-011-9527-9.
(55) Amber Home Page; http://ambermd.org (accessed June 12, 2011).
(56) Frisch, M. J.; Trucks, G. W.; Schlegel, H. B.; Scuseria, G. E.; Robb, M. A.; Cheeseman, J. R.; Scalmani, G.; Barone, V.; Mennucci, B.; Petersson, G. A.; Nakatsuji, H.; Caricato, M.; Li, X.; Hratchian, H. P.; Izmaylov, A. F.; Bloino, J.; Zheng, G.; Sonnenberg, J. L.; Hada, M.; Ehara, M.; Toyota, K.; Fukuda, R.; Hasegawa, J.; Ishida, M.; Nakajima, T.; Honda, Y.; Kitao, O.; Nakai, H.; Vreven, T.; Montgomery, J. A., Jr.; Peralta, J. E.; Ogliaro, F.; Bearpark, M.; Heyd, J. J.; Brothers, E.; Kudin, K. N.; Staroverov, V. N.; Kobayashi, R.; Normand, J.; Raghavachari, K.; Rendell, A.; Burant, J. C.; Iyengar, S. S.; Tomasi, J.; Cossi, M.; Rega, N.; Millam, J. M.; Klene, M.; Knox, J. E.; Cross, J. B.; Bakken, V.; Adamo, C.; Jaramillo, J.; Gomperts, R.; Stratmann, R. E.; Yazyev, O.; Austin, A. J.; Cammi, R.; Pomelli, C.; Ochterski, J. W.; Martin, R. L.; Morokuma, K.; Zakrzewski, V. G.; Voth, G. A.; Salvador, P.; Dannenberg, J. J.; Dapprich, S.; Daniels, A. D.; Farkas, Ö.; Foresman, J. B.; Ortiz, J. V.; Cioslowski, J.; Fox, D. J. *Gaussian 09*; Gaussian, Inc.: Wallingford, CT, 2009.
(57) Frisch, M. J.; Trucks, G. W.; Schlegel, H. B.; Scuseria, G. E.; Robb, M. A.; Cheeseman, J. R.; Montgomery, J. A., Jr.; Vreven, T.; Kudin, K. N.; Burant, J. C.; Millam, J. M.; Iyengar, S. S.; Tomasi, J.; Barone, V.; Mennucci, B.; Cossi, M.; Scalmani, G.; Rega, N.; Petersson, G. A.; Nakatsuji, H.; Hada, M.; Ehara, M.; Toyota, K.; Fukuda, R.; Hasegawa, J.; Ishida, M.; Nakajima, T.; Honda, Y.; Kitao, O.; Nakai, H.; Klene, M.; Li, X.; Knox, J. E.; Hratchian, H. P.; Cross, J. B.; Bakken, V.; Adamo, C.; Jaramillo, J.; Gomperts, R.; Stratmann, R. E.; Yazyev, O.; Austin, A. J.; Cammi, R.; Pomelli, C.; Ochterski, J. W.; Ayala, P. Y.; Morokuma, K.; Voth, G. A.; Salvador, P.; Dannenberg, J. J.; Zakrzewski, V. G.; Dapprich, S.; Daniels, A. D.; Strain, M. C.; Farkas, O.; Malick, D. K.; Rabuck, A. D.; Raghavachari, K.; Foresman, J. B.; Ortiz, J. V.; Cui, Q.; Baboul, A. G.; Clifford, S.; Cioslowski, J.; Stefanov, B. B.; Liu, G.; Liashenko, A.; Piskorz, P.; Komaromi, I.; Martin, R. L.; Fox, D. J.; Keith, T.; Al-Laham, M. A.; Peng, C. Y.; Nanayakkara, A.; Challacombe, M.; Gill, P. M. W.; Johnson, B.; Chen, W.; Wong, M. W.; Gonzalez, C.; Pople, J. A. *Gaussian 03*; Gaussian, Inc.: Wallingford, CT, 2004.
(58) *Jaguar, version 7.8*; Schrödinger, LLC: New York, 2011.
(59) Jorgensen, W. L.; Chandrasekhar, J.; Madura, J. D.; Impey, R. W.; Klein, M. L. *J. Chem. Phys.* **1983**, *79*, 926−935.
(60) Martyna, G. J.; Tobias, D. J.; Klein, M. L. *J. Chem. Phys.* **1994**, *101*, 4177−4189.
(61) Darden, T.; York, D.; Pedersen, L. *J. Chem. Phys.* **1993**, *98*, 10089−10092.
(62) Chou, K. *Anal. Biochem.* **2000**, *286*, 1−16.
(63) Ramachandran, G. N.; Ramakrishnan, C.; Sasisekharan, V. *J. Mol. Biol.* **1963**, *7*, 95−99.
(64) Katritzky, A. R.; Soti, F. *J. Chem. Soc., Perkin Trans. 1* **1974**, 1427−1432.